

## A combined voxel-based morphometry and $^1\text{H}$ -MRS study in patients with Friedreich's ataxia

Marcondes C. França Jr · Anelyssa D'Abreu · Clarissa L. Yasuda ·  
Luciana Cardoso Bonadia · Marilza Santos da Silva · Anamarli Nucci ·  
Ischia Lopes-Cendes · Fernando Cendes

Received: 23 June 2008 / Revised: 25 January 2009 / Accepted: 12 February 2009 / Published online: 12 March 2009  
© Springer-Verlag 2009

**Abstract** Friedreich's ataxia (FA) is the most frequent autosomal recessive ataxia and essentially considered a disease of the dorsal root ganglia and spinal cord. It is caused by homozygous GAA expansions in the Frataxin gene in most cases. Although only a few studies have addressed cerebral involvement in FA, cognitive symptoms have lately been emphasized. To evaluate brain damage in vivo, we employed whole-brain VBM and analysis of pre-defined regions of interest (ROIs) over the cerebellum to compare 24 patients with 24 age-and-sex-matched normal controls.  $^1\text{H}$ -MRS of deep cerebral white matter (WM) was subsequently performed. Mean age of patients was 28 years (range 14–45), mean duration of disease was 14 years (range 5–28) and 11 were men. Mean length of shorter (GAA1) and longer (GAA2) alleles were 735 and 863, respectively. VBM analysis identified WM atrophy in the posterior cingulate gyrus, paracentral lobule and middle frontal gyrus. ROIs over the infero-medial cerebellar hemispheres and dorsal brainstem presented gray matter atrophy, which correlated with duration of disease ( $r =$

$-0.4$ ). NAA/Cr ratios were smaller among patients ( $P = 0.006$ ), but not Cho/Cr ( $P = 0.08$ ). Our results provide evidence of axonal damage in the cerebellum, brainstem and subcortical WM in FA. This suggests that neuronal dysfunction is more widespread than previously thought in FA.

**Keywords** Friedreich's ataxia · Voxel-based morphometry · Magnetic resonance spectroscopy · Cerebral white matter

### Introduction

Friedreich's ataxia (FA) is the most common inherited ataxia overall, with prevalence rates ranging from 1:30.000 to 1:50.000 [14]. It is an autosomal recessive condition which is caused in 96% of cases by a homozygous triplet GAA expansion in the first intron of the *Frataxin* (*FXN*) gene on chromosome 9q13 [7]. The disease typically begins before 25 years of age and is characterized by progressive ataxia, deep sensory abnormalities, 'pes cavus', scoliosis, cardiomyopathy, diabetes, and gaze abnormalities [12].

FA is essentially considered a disease of the dorsal root ganglia, peripheral nerves, spinal cord and cerebellum [12]. Few studies addressed cerebral involvement in the disease [13, 18]. Despite this, symptoms not related to the ataxic syndrome itself, such as psychomotor slowing and executive dysfunction, have been increasingly recognized [8, 21, 31].

We aimed to evaluate the presence and extent of cerebral damage in patients with FA using two neuroimaging modalities, MRI voxel-based morphometry (VBM) and proton magnetic resonance spectroscopy ( $^1\text{H}$ -MRS). VBM

---

M. C. França Jr · A. D'Abreu · C. L. Yasuda · A. Nucci ·  
F. Cendes  
Department of Neurology, University of Campinas (UNICAMP),  
Campinas, Sao Paulo, Brazil  
e-mail: mcfrancajr@uol.com.br

L. C. Bonadia · M. Santos da Silva · I. Lopes-Cendes  
Department of Medical Genetics,  
University of Campinas (UNICAMP),  
Campinas, Sao Paulo, Brazil

F. Cendes (✉)  
Department of Neurology, Universidade Estadual de Campinas,  
UNICAMP. Cidade Universitaria "Zeferino Vaz",  
Campinas, SP 13083-970, Brazil  
e-mail: fcendes@unicamp.br

is an automated unbiased method used to assess structural changes in 3-D MRI, which has been successfully employed to investigate several neurodegenerative diseases [2]. <sup>1</sup>H-MRS can quantify neuronal damage or dysfunction in vivo by measuring the levels of several neurometabolites in different regions of central nervous system [26].

## Methods

### Subject selection

Twenty four patients with molecular confirmation of FA and prospectively followed in the neurogenetics outpatient clinic of University of Campinas (UNICAMP) were included in the final VBM analysis. Clinical (sex, age at disease onset, duration of disease, clinical subtype) and genetic data (length of expanded repeat in both shorter, GAA1, and longer, GAA2, alleles) were recorded. Severity of ataxia was quantified with Friedreich's ataxia rating scale (FARS) [28].

Mean age of patients was 28 years (range 14–45), mean duration of disease was 14 years (range 5–28) and 11 were men. Mean length of GAA1 and GAA2 alleles were 735 and 863, respectively. Eighteen patients had typical FA, five had FA with retained reflexes and one late-onset FA. Diabetes mellitus and cardiac disease were found in six and five individuals, respectively. All but one had kypho-scoliosis. Mean FARS score was 90.5 (SD = 23.5). Twenty four healthy controls were age and sex-matched to patients (mean age = 28 years and 11 men).

Patients with autosomal recessive cerebellar ataxia but no molecular confirmation of FA were not included. Individuals unable to perform MRI or with significant motion artifacts on scans were not included in the final analysis. Imaging findings were compared to a normal control group of age and sex-matched individuals. These were mostly physicians and employees at UNICAMP Hospital and were recruited along the study period. This study was approved by our institution ethics committee and a written informed consent was obtained from all participants.

### VBM protocol and analysis

All FA patients and controls had MRI scans using an Elscint Prestige 2T scanner (Haifa, Israel). T1- and T2-weighted images were acquired in axial, coronal, and sagittal planes with thin cuts. In addition, volumetric (3D) T1 gradient echo (GRE) images were acquired in the sagittal plane with 1 mm thickness (flip angle = 35°, time to repeat = 22 ms, echo time = 9 ms, matrix = 256 × 220, field of view = 23 × 25 cm). These images were

used for VBM analysis. All images underwent visual analysis by two independent investigators (MCFJ and AD).

MRI scans produce images in DICOM format. These images were converted into ANALYSE format using the MRIcro software ([www.mricro.com](http://www.mricro.com)). As described elsewhere [16], we used SPM2 software (Wellcome Department of Imaging Neuroscience, London, England; [www.fil.ion.ucl.ac.uk](http://www.fil.ion.ucl.ac.uk)) on MATLAB 7.0 to perform several fully automated imaging pre-processing steps, including spatial normalization of all images to the same stereotaxic space, segmentation into white and gray matter and cerebrospinal fluid compartments, correction for volume changes induced by spatial normalization (modulation) and smoothing. Spatial normalization was performed by matching the individual's image to a standard template by estimating the optimum 12-parameter affine transformation to correct for global brain shape differences [2]. The spatially normalized images were then partitioned into gray matter (GM), white matter (WM) and cerebrospinal fluid by using segmentation in-built SPM2 routines. Images were modulated to correct for spatial deformation induced by normalization [16]. Segmented WM and GM modulated images were smoothed with a 10-mm full width at half maximum (FWHM) Isotropic Gaussian Kernel, rendering the data more normally distributed.

Processed images of patients and controls were compared using a voxel-wise statistical analysis. We looked for differences in WM and GM volumes between the two groups. The statistical analysis for all comparisons was performed with grand mean scaling, proportional threshold masking (0.8) and implicit masking. We defined the contrast searching for areas of reduced and increased GM concentration as well as WM concentration. The results were corrected for multiple comparisons using a false discovery rate (FDR) of 5% [15] and significant differences set at  $P < 0.05$ .

We also performed statistical analysis of regions of interest (ROI) over the cerebellum. ROIs provide increased statistical power over voxel-by-voxel analyses because the number of comparisons is tremendously reduced [4]. We used the software MARSbar ([www.marsbar.sourceforge.net](http://www.marsbar.sourceforge.net)) to extract mean GM and WM volumes of these cerebellar ROIs, whose boundaries were based on the automatic anatomic labeling (AAL) ROI library [27, 29]. According to this library, cerebellar hemispheres are divided into nine regions and vermis into eight regions. We used SPM-2 to perform two sample *t* tests to compare mean ROI volumes in patients and controls. Statistical significance was considered at  $P < 0.05$  without Bonferroni correction for multiple comparisons. Volumes were then correlated with age at onset, duration of disease, length of expanded (GAA)<sub>1</sub> and FARS score, by linear regression

(with Bonferroni probabilities) on SYSTAT 10.2 (SSI, San Jose, California).

### MRS protocol and analysis

We attempted to characterize additional evidence of the cerebral white matter abnormality by using MRS with the ROI centered in the region indicated by VBM analysis. We acquired single voxel  $^1\text{H}$ -MRS using point resolved spectroscopy (PRESS) sequence [5] with TR = 1,500 ms, TE = 135 ms, NEX = 200, over the superior–posterior region of the right hemisphere at the level of the corpus callosum. We placed one single voxel ( $5 \times 2 \times 1$  cm) over the ROI, after the acquisition of scout anatomical images in sagittal planes for localization of corpus callosum [1]. Prior to the acquisition, we performed a localized shimming at the ROI to ensure adequate field homogeneity followed by water suppression adjustment.

The spectra were post-processed using software supplied by the machine manufacturer (Elscent 2T Prestige, Haifa, Israel). After zero-filling and baseline correction we determined peak areas by integration of the corresponding signals from *N*-acetyl compounds (NAA) at 2.01 ppm, choline-based compounds (Cho) at 3.2 ppm and creatine and phosphocreatine containing compounds (Cr) at 3.0 ppm. We scaled the spectra in relation to creatine values. NAA/Cr and Cho/Cr ratios were used for analyses. Two investigators (MCFJ and AD) performed the spectral acquisition, quantification and analysis. The evaluation was cross-checked by one spectroscopist (FC). These investigators judged independently the quality of the spectral analysis. We excluded from analysis the spectra with broad peaks, poor separation of individual peaks and poor signal to noise ratio judged by the spectra baseline. We employed Student's *t* test to compare NAA/Cr and Cho/Cr ratios between the FA and control groups. *P* values < 0.05 were considered significant.

### Results

On whole-brain VBM analysis, we did not find significant encephalic GM volumetric reduction. However, we found loss of WM in the posterior cingulate gyrus (Talairach coordinates  $x = -15$ ,  $y = -34$ ,  $z = 28$ ), middle frontal gyrus ( $x = -11$ ,  $y = -8$ ,  $z = 67$ ) and paracentral lobule ( $x = -13$ ,  $y = -25$ ,  $z = 52$ ). These areas with significant volume loss were symmetric and involved periventricular regions (Fig. 1 and Table 1). There were no areas of white matter volume increase in patients with FA.

Analysis of ROIs (without Bonferroni correction for multiple comparisons) identified reduced GM volumes (Fig. 2) in the infero-medial portions of cerebellar

hemispheres ( $P = 0.006$ ), as well as dorsal pons ( $P = 0.001$ ) and dorsal midbrain with superior cerebellar peduncles ( $P = 0.019$ ). In addition, there was WM volumetric reduction in the infero-medial portions of cerebellar hemispheres ( $P = 0.018$ ), and rostral vermis ( $P = 0.005$ ) (Fig. 3). Posterior cingulate WM volumes did not correlate with age at examination ( $P = 0.105$ ) or duration of disease ( $P = 0.212$ ). GM volumes in the infero-medial portions of cerebellar hemispheres were related to duration of disease ( $r = -0.40$ ,  $P = 0.05$ ). WM volumes in rostral vermis (regions 6, 7 and 8 in the automatic anatomic labeling package) also showed an inverse correlation with duration of disease ( $r = -0.39$ ,  $P = 0.05$ ). None of the volumes showed significant association with GAA1 length or FARS score.

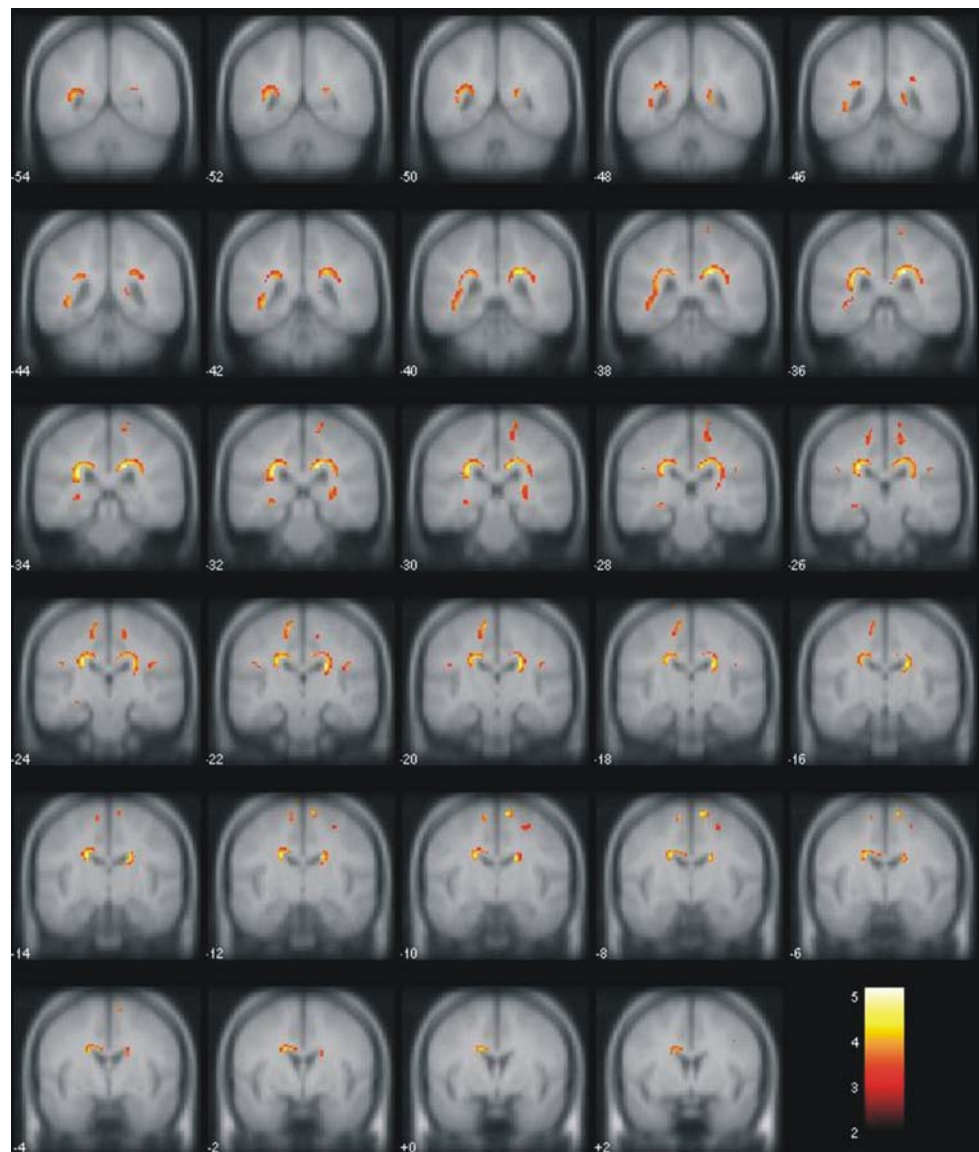
Twenty out of the 24 patients underwent  $^1\text{H}$ -MRS analysis (two were unable to perform MRS scans and two were excluded due to poor quality spectra). We found significant differences of NAA/Cr ( $1.65 \pm 0.33 \times 1.83 \pm 0.51$ ,  $P = 0.009$ ), but not Cho/Cr ( $0.93 \pm 0.18 \times 0.98 \pm 0.12$ ,  $P = 0.16$ ) ratios between patients and controls. We did not detect lactate peaks above baseline in patients with FA.

### Discussion

Previous neuroimaging studies in FA emphasized cervical spinal cord abnormalities (antero-posterior volumetric reduction with hyperintense T2 lesions restricted to dorsal funiculi) with relatively preserved cerebellar volumes [11, 22, 25, 30, 32]. Significant damage to cerebral hemispheres was not recognized in patients with FA, possibly because investigators focused in the anatomic structures more obviously implicated in the phenotype. Some of these studies, however, were performed before the identification of the *FXN* mutation [11, 22, 25, 30, 32], included few patients [22, 32] or employed inaccurate neuroimaging techniques [30, 32].

Although whole-brain VBM has been successfully employed to evaluate structural damage in several neurodegenerative diseases [6, 20, 27], the method appears to be less sensitive to detect subtle abnormalities in the posterior cranial fossa [9]. We therefore attempted to overcome this limitation by using analysis of pre-defined ROIs over brainstem and cerebellum in addition to whole-brain VBM. This provides increased statistical power over voxel-by-voxel analyses because the number of comparisons is tremendously reduced [4]. On whole-brain VBM analysis, we found volumetric reduction of deep WM adjacent to posterior ventricles, which include associative fibers and tracts. Analysis of ROIs showed volumetric reduction of GM in the infero-medial portions of cerebellar hemispheres

**Fig. 1** Results of whole brain parametric voxelwise analysis comparing 24 patients with FA and 24 age-and-sex matched controls. The areas of significant white matter atrophy are overlaid in a smoothed anatomical template. The color-coded bar represent the Z-score



and dorsal brainstem, as well as WM volumetric reduction in the infero-medial portions of cerebellar hemispheres and vermis.

These results are partly in agreement with a recently published VBM study in FA [9]. Regions of reduced GM and WM in posterior cranial fossa identified in both studies are similar. However, two relevant differences must be discussed at this point. In contrast to Della Nave et al., we were not able to identify these abnormalities in posterior fossa using only whole-brain VBM. This is probably due to the older age of patients in the former study (mean age of 33 vs. 25 years), and thus longer disease duration and more severe atrophy. The second difference regards deep WM damage which was not found by the Della Nave et al. [9]. Patients and controls were neither sex nor age-matched in

that study, and such small discrepancies may be relevant in VBM studies with small samples (20 patients).

The atrophic areas on posterior cranial fossa match previous pathological descriptions [19, 24]. WM gliosis may account for the vermian and infero-medial cerebellar atrophy [24]. Degeneration of gracilis and cuneatus fasciculi leads to shrinkage of the respective nuclei and projections in the dorsal brainstem; this may be the anatomic correlate of GM atrophy in the dorsal medulla, pons and midbrain. Supratentorial involvement has been occasionally reported in pathology and neuroimaging studies. Mild but consistent neuropathologic abnormalities have been identified in the cerebral hemispheres of patients with FA [19, 24]. Several authors described depletion of cortical Betz cells [19, 24]; other findings such as neuronal loss in

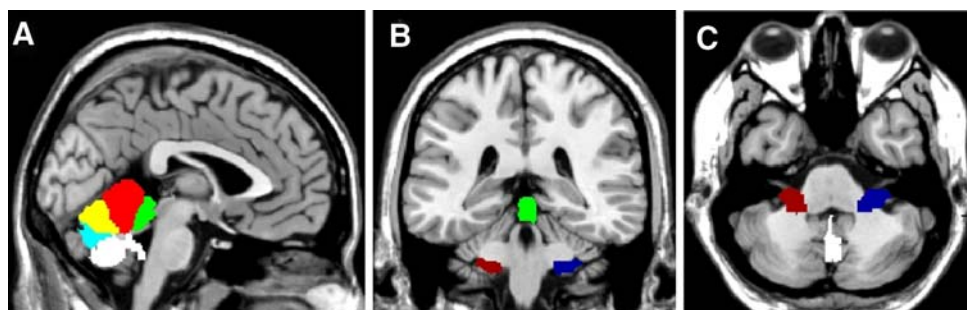


**Table 1** Areas of WM atrophy in patients with Friedreich ataxia identified on whole brain VBM analysis

Cluster	Cluster size	P (FDR-cor)	T	Z-score	X, Y, Z {mm}MNI coordinates	Anatomic location
1	9994	0.016	5.2	4.58	-19 -16 25	L cyngulate gyrus
		0.016	5.13	4.54	-16 -34 28	L sub-gyral
		0.016	4.57	4.13	-23 -23 26	
2	11711	0.016	5.11	4.53	26 -31 25	R cyngulate gyrus
		0.016	4.91	4.38	19 -11 26	R sub-gyral
		0.016	4.85	4.33	23 -23 27	
3	3482	0.016	4.6	4.15	-11 -8 67	L medial frontal gyrus
		0.017	4.03	3.71	-16 -30 68	L middle frontal gyrus
		0.02	3.76	3.49	-13 -26 52	L precentral gyrus
4	1060	0.016	4.48	4.06	-37 10 41	L middle frontal gyrus
		0.024	3.54	3.31	-40 3 36	L inferior frontal gyrus
5	2489	0.016	4.29	3.91	11 -21 58	R medial frontal gyrus
		0.016	4.13	3.79	9 -10 63	R sub-gyral
		0.037	3.1	2.94	15 -31 65	
6	158	0.016	4.22	3.86	-20 -74 -4	L lingual gyrus
		0.031	3.26	3.07	-26 -69 -2	
7	404	0.021	3.7	3.44	-42 -64 -8	L inferior temporal gyrus
						L sub-gyral
8	621	0.022	3.66	3.41	42 -23 23	R inferior parietal lobule
9	542	0.025	3.5	3.28	39 -77 -8	R middle occipital gyrus
		0.031	3.26	3.08	45 -71 1	R inferior occipital gyrus
10	846	0.029	3.33	3.13	48 14 15	R inferior frontal gyrus
		0.034	3.18	3	41 6 31	R sub-gyral
11	263	0.03	3.3	3.11	-35 -39 -2	L temporal lobe, sub-gyral
		0.033	3.22	3.04	-40 -28 -12	
12	177	0.031	3.26	3.08	37 -1 13	R insula
		0.044	2.91	2.77	40 -9 18	
13	415	0.032	3.23	3.05	-42 3 21	L insula
		0.041	2.98	2.84	-40 -4 17	L sub-gyral
14	104	0.036	3.12	2.95	-19 -63 31	L precuneus

Result reported on Height threshold:  $T = 2.91$ , FDR (0.05), clusters > 100 voxels

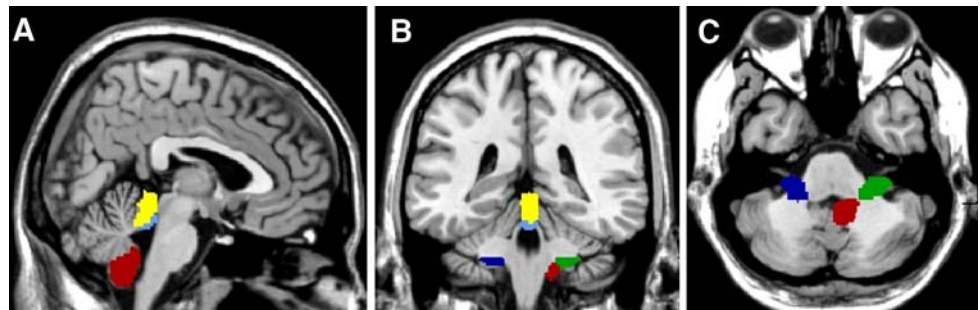
**Fig. 2** ROIs with reduced gray matter volumes identified on non-parametric analysis. **a** Sagittal view. **b** Coronal view. **c** Axial view. Each one of these ROIs is represented with a different color only for display purposes



the thalamus and pallor of optic tracts have been also reported [19, 24]. Previous neuroimaging reports also support our findings. A CT and PET study found widespread cerebral atrophy in addition to reduced cerebral metabolic rates in patients with FA [18]. In those

individuals, atrophy was especially severe in periventricular regions, as seen in our patients. Deep cerebral damage in FA was recently described by Della nave et al. using tract-based spatial statistics; atrophic regions were similar to those we found [10].

**Fig. 3** ROIs with reduced white matter volumes identified on non-parametric analysis. **a** Sagittal view. **b** Coronal view. **c** Axial view



We tried to further characterize deep cerebral WM damage with  $^1\text{H}$ -MRS. We identified reduced NAA/Cr levels in the region thus confirming the axonal damage in FA. Amounting evidence indicates that NAA is synthesized in neurons inside mitochondria [23]. Therefore, the reduced expression of *FXN* in FA, which interferes with mitochondrial function possibly due to the accumulation of iron-bound free radicals, might explain, at least in part, such reduction of NAA [3]. In contrast, lactate peaks, which are another usual finding in diseases with mitochondrial compromise, were not detected above baseline in our patients.

Volumetric reductions of infero-medial regions of cerebellar hemispheres and rostral vermis were associated with duration of disease, which suggest that these truly reflect atrophy evolving along the disease course. However, posterior cingulate WM volume reduction did not show a similar association. We hypothesize that the mechanism underlying cerebral damage is different. In adult humans, *FXN* is widely expressed in dorsal root ganglia and spinal cord neurons, but not in cerebral cortex [7]. In the mouse model, however, there is marked cerebral expression of the protein during embryogenesis, especially in the proliferating neural precursors of the periventricular zone [17]. Given the high overlap of human and mouse *FXN* tissue expression, the former pattern might also be found in humans and this would explain the selective damage to periventricular WM. In this context, it is possible that the cerebral volumetric reduction we found is a developmental problem rather than true atrophy.

In conclusion, we have employed VBM analyses to show that some infratentorial structures are atrophic in patients with FA. We also provided  $^1\text{H}$ -MRS evidence of axonal damage in the normal appearing deep cerebral WM of these patients. These findings widen the phenotypic spectrum of the disease and suggest that neuronal damage is more widespread than previously thought in FA.

**Acknowledgments** Supported by a grant from Fundação de Amparo à Pesquisa do Estado de São Paulo – FAPESP, São Paulo, Brazil, Grant # 04/13725-4.

## References

- Appenzeller S, Li LM, Costallat LT, Cendes F (2005) Evidence of reversible axonal dysfunction in systemic lupus erythematosus: a proton MRS study. *Brain* 128:2933–2940
- Ashburner J, Friston KJ (2000) Voxel-based morphometry—the methods. *Neuroimage* 11:805–821
- Babady NE, Carelle N, Wells RD et al (2007) Advancements in the pathophysiology of Friedreich’s Ataxia and new prospects for treatments. *Mol Genet Metab* 92:23–35
- Bonilha L, Rorden C, Appenzeller S, Coan AC, Cendes F, Li LM (2006) Gray matter Atrophy associated with duration of temporal lobe epilepsy. *Neuroimage* 32:1070–1079
- Bottomley PA (1987) Spatial localization in NMR spectroscopy in vivo. *Ann NY Acad Sci* 508:333–348
- Brenneis C, Boesch SM, Egger KE et al (2006) Cortical atrophy in the cerebellar variant of multiple system atrophy: a voxel-based morphometry study. *Mov Disord* 21:159–165
- Campuzano V, Montermini L, Molto MD et al (1996) Friedreich’s ataxia: autosomal recessive disease caused by an intronic GAA triplet repeat expansion. *Science* 271:1423–1427
- Corben LA, Georgiou-Karistianis N, Fahey MC et al (2006) Towards an understanding of cognitive function in Friedreich ataxia. *Brain Res Bull* 70:197–202
- Della Nave R, Ginestroni A, Giannelli M et al (2008) Brain structural damage in Friedreich ataxia. *J Neurol Neurosurg Psychiatry* 79:82–85
- Della Nave R, Ginestroni A, Tessa C et al (2008) Brain white matter tracts degeneration in Friedreich ataxia an in vivo MRI study using tract-based spatial statistics and voxel-based morphometry. *Neuroimage* 40:19–25
- De Michele G, Di Salle F, Filla A et al (1995) Magnetic resonance imaging in “typical” and “late onset” Friedreich’s disease and early onset cerebellar ataxia with retained tendon reflexes. *Ital J Neurol Sci* 16:303–308
- Durr A, Cossee M, Agid Y et al (1996) Clinical and genetic abnormalities in patients with Friedreich’s ataxia. *N Engl J Med* 335:1169–1175
- Eder K, Kish SJ, Kirchgessner M, Ross BM (1998) Brain phospholipids and fatty acids in Friedreich’s ataxia and spinocerebellar atrophy type-1. *Mov Disord* 13:813–819
- Fogel BL, Perlman S (2007) Clinical features and molecular genetics of autosomal recessive cerebellar ataxias. *Lancet Neurol* 6:245–257
- Genovese CR, Lazar NA, Nichols T (2002) Thresholding of statistical maps in functional neuroimaging using the false discovery rate. *Neuroimage* 15:870–878
- Good CD, Johnsrude IS, Ashburner J, Henson RNA, Friston KJ, Frackowiak RSJ (2001) A voxel-based morphometric study of ageing in 465 normal adult human brains. *Neuroimage* 14:21–36

17. Jiralerspong S, Liu Y, Montermini L, Stifani S, Pandolfo M (1997) Frataxin shows developmentally regulated tissue-specific expression in the mouse embryo. *Neurobiol Dis* 4:103–113
18. Junck L, Gilman S, Gebarski SS, Koeppe RA, Kluin KJ, Markel DS (1994) Structural and functional brain imaging in Friedreich's ataxia. *Arch Neurol* 51:349–355
19. Lamarche JB, Lemieux B, Lieu HB (1984) The neuropathology of "typical" Friedreich's ataxia in Quebec. *Can J Neurol Sci* 11:592–600
20. Lasek K, Lencer R, Gaser C et al (2006) Morphological basis for the spectrum of clinical deficits in spinocerebellar ataxia 17 (SCA17). *Brain* 129:2341–2352
21. Mantovan MC, Martinuzzi A, Squarzanti F et al (2006) Exploring mental status in Friedreich's ataxia: a combined neuropsychological, behavioral and neuroimaging study. *Eur J Neurol* 13:827–835
22. Mascalchi M, Salvi F, Piacentini S, Bartolozzi C (1994) Friedreich's ataxia: MR findings involving the cervical portion of the spinal cord. *AJR Am J Roentgenol* 163:187–191
23. Moffett JR, Ross B, Arun P, Madhavarao CN, Namboodiri AM (2007) *N*-Acetylaspartate in the CNS: from neurodiagnostics to neurobiology. *Prog Neurobiol* 8:89–131
24. Oppenheimer DR (1979) Brain lesions in Friedreich's ataxia. *Can J Neurol Sci* 6:173–176
25. Ormerod IE, Harding AE, Miller DH et al (1994) Magnetic resonance imaging in degenerative ataxic disorders. *J Neurol Neurosurg Psychiatry* 57:51–57
26. Rudkin TM, Arnold DL (1999) Proton magnetic resonance spectroscopy for the diagnosis and management of cerebral disorders. *Arch Neurol* 56:919–926
27. Ruocco HH, Bonilha L, Li LM, Lopes-Cendes I, Cendes F (2008) Longitudinal analysis of regional gray matter loss in Huntington disease: effects of the length of the CAG repeat. *J Neurol Neurosurg Psychiatry* 79:130–135
28. Subramony SH, May W, Lynch D et al (2005) Cooperative Ataxia Group measuring Friedreich ataxia: interrater reliability of a neurologic rating scale. *Neurology* 64:1261–1262
29. Tzourio-Mazoyer N, Landeau B, Papathanassiou D et al (2002) Automated anatomical labeling of activations in SPM using a macroscopic anatomical parcellation of the MNI MRI single-subject brain. *Neuroimage* 15:273–289
30. Wessel K, Schroth G, Diener HC, Muller-Forell W, Dichgans J (1989) Significance of MRI-confirmed atrophy of the cranial spinal cord in Friedreich's ataxia. *Eur Arch Psychiatry Neurol Sci* 238:225–230
31. White M, Lalonde R, Botez-Marquard T (2000) Neuropsychologic and neuropsychiatric characteristics of patients with Friedreich's ataxia. *Acta Neurol Scand* 102:222–226
32. Wullner U, Klockgether T, Petersen D, Naegele T, Dichgans J (1993) Magnetic resonance imaging in hereditary and idiopathic ataxia. *Neurology* 43:318–325